AD-A159 534 CONTRIBUTIONS TO THE INTERNATIONAL ACOUSTIC EMISSION CONFERENCE (2ND)(U) CALIFORNIA UNIV LOS ANGELES DEPT OF MATERIALS SCIENCE AND ENG.. C JOHNSON ET AL. SEP 85 1/1

UNCLASSIFIED TR-85-1 N00014-81-K-0011 F/G 20/1 NL

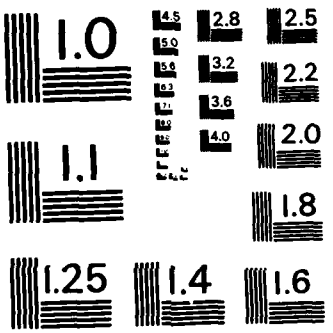

SECURITY CLASSIFICATION OF THIS PAGE (When Data Entered)

REPORT DOCUMENTATION PAGE

READ INSTRUCTIONS BEFORE COMPLETING FORM

1 REPORT NUMBER: 85-1	2 GOVT ACCESSION NO.: AD-A159534
3 RECIPIENT'S CATALOG NUMBER:	
4 TITLE (and Subtitle): Contributions to the Second International Acoustic Emission Conference	5 TYPE OF REPORT & PERIOD COVERED: Technical
	6 PERFORMING ORG REPORT NUMBER:
7 AUTHOR(s): C. Johnson, M. Ohtsu, O.Y. Kwon, D. Chellman K. Ono and I. Roman	8 CONTRACT OR GRANT NUMBER(s): N00014-81-K-0011
9 PERFORMING ORGANIZATION NAME AND ADDRESS: Materials Science and Engineering Department 6532 Boelter Hall, Univeristy of California Los Angeles, CA 90024	10 PROGRAM ELEMENT, PROJECT, TASK AREA & WORK UNIT NUMBERS: 61153N RR011-08-01 NR 384-700
11 CONTROLLING OFFICE NAME AND ADDRESS: Physics Division Code 412 ONR-800 North Quincy Street Arlington, Virginia 22217	12 REPORT DATE: September 1985 13 NUMBER OF PAGES: 21
14 MONITORING AGENCY NAME & ADDRESS (if different from Controlling Office)	15 SECURITY CLASS (of this report): Unclassified 15a DECLASSIFICATION DOWNGRADING SCHEDULE

16 DISTRIBUTION STATEMENT (of this Report)

Unlimited

DISTRIBUTION STATEMENT A
Approved for public release
Distribution Unlimited

Reproduction in whole in part is permitted for any purpose of the U.S. Government

17 DISTRIBUTION STATEMENT (of the abstract entered in Block 20, if different from Report)

18 SUPPLEMENTARY NOTES

DTIC ELECTE SEP 25 1985 S B D

19 KEY WORDS (Continue on reverse side if necessary and identify by block number)

Acoustic Emission
Metal Matrix Composites
Structural Steels
Aluminum-Lithium Alloy
Pattern Recognition Analysis

20 ABSTRACT (Continue on reverse side if necessary and identify by block number)

This report is a compilation of four extended abstracts to be presented at the 2nd International Conference on Acoustic Emission at Lake Tahoe, on 28 October to 1 November 1985. The abstracts include information about the [illegible]

DD FORM 1 JAN 73 1473

SECURITY CLASSIFICATION OF THIS PAGE (When Data Entered)

AD-A159 534

DTIC FILE COPY

Cont'd

Discrimination of Fracture Mechanisms via Pattern Recognition Analysis of (AE) Signals during Fracture Testing

Acoustic Emission

Kanji Ono and Masayasu Ohtsu*
Department of Materials Science and Engineering
University of California, Los Angeles, Calif. 90024

*Permanent Address: Kumamoto University, Kumamoto, Japan

Introduction

In recent years, there has been a considerable growth of interest in problems of pattern recognition. Pattern recognition has been used in a variety of fields, including acoustic emission signal analysis /1-3/. In speech analysis ,the autoregressive modeling has been employed successfully for pattern recognition of human voice /4/. Autoregressive modeling is also applicable to acoustic emission analysis. The application of this approach to classify AE waveforms was explored with moderate success /5/. Utilizing autoregressive modeling, this work demonstrates the feasibility of classifying AE waveforms of ASTM A533B steel specimens undergoing fracture.

Methods of Pattern Recognition

Mathematical techniques used to solve pattern recognition problems are classified into two general approaches. These are decision-theoretic and syntactic approaches. Most of the developments in pattern recognition research during the past decade have dealt with the decision-theoretic approach /6/. Here, a set of characteristic measurements, namely "features," are extracted from each grouping of measured data. For example, a digital AE signal recognition system receives a digitized AE waveform as an input, evaluates a set of features for the input, and then classifies the waveform based on the values of the features to one of several predetermined patterns.

The most important problem is the criteria of making decision on the class assignment to predetermined patterns. A simple and important class of linear classifiers is called the nearest neighbor classifier. It employs the distance between the features of an input pattern and a reference in the vector space. A set of features usually consists of numerical values and can be referred to as a vector in the multi-dimensional vector space. The classifier assigns an input datum to one of the reference patterns, which is associated with the closest vector. This concept can be extended to multi-component data. The rule identifies the input data with the class of its nearest neighbor, where nearness are measured by Euclidean distance,

$$\text{Distance}(x,r) = ((x_1-r_1)^2+\ldots+(x_i-r_i)^2+\ldots+(x_n-r_n)^2)^{1/2} = \left(\sum_i (x_i-r_i)^2\right)^{1/2} \quad (1)$$

where $x = (x_1,..x_i..,x_n)$ is the input vector and $r = (r_1,..r_i,...,r_n)$ is the reference vector. These elements of the vectors consist of the features of patterns.

Autoregressive Modeling

In several pattern recognition systems, autoregressive coefficients have been successfully employed as features of pattern classification. The concept of autoregressive modeling is derived from the z-transform of a discrete sequence. The filter coefficients are known as the autoregressive coefficients; they are also referred to as the linear predictive coefficients or the maximum entropy coefficients /7/.

Given a set of autoregressive coefficients, we can find frequency responses H(f) of an autoregressive model by,

$$H(f) = G/A(f), \tag{2}$$

where $A(f) = 1 - \sum_i a_i \exp(- j2\pi ifT)$. Here, f is frequency, A(f) is the characteristics of an inverse filter, a_i are the autoregressive coefficients, G is a gain of the system, T is a sampling interval, and $j^2 = -1$, respectively. It is known that if the number of coefficients n is large enough, we can approximate any signal spectrum by H(f) within an arbitrarily small error. This model is also known as an all-pole filter with poles inside a unit circle. Spectrum H(f) mathematically agrees with the power spectrum of the waveform much more closely in the regions of large signal energy than near the regions of low signal energy. This is due to the fact that the coefficients are usually determined by minimizing the mean-square error between the power spectrum and the frequency response of the model. The regions of large signal energy contribute more to the total error than the regions of low energy. Therefore, the spectrum modeled by equation 2 shows a good fit near the peaks of the power spectrum, whereas the fit near the spectral valley is poor.

AE Data Acquisition and Analysis

We employed ASTM A533B class 1 steel specimens of dimensions 10 mm x 10 mm x 55 mm with a 2 mm deep V notch. It has the chemical composition of 0.18 C, 0.25 Si, 1.43 Mn, 0.013 P, 0.005 S, 0.50 Mo, 0.66 Ni, 0.28 Cr, and 0.01 Cu. The specimens were austenitized at 940°C for one hour and quenched into water.

A sample was placed in a three-point bending jig on an Instron and loaded to fracture. During loading, AE data were collected from several different regions of load-displacement curves. Other samples were then loaded to corresponding stages for the purpose of getting fractographs of various stages of crack growth /8/. AE signals were detected by a wideband transducer (Model 10-2-3, NSC), because this transducer was well characterized. Detected signals were amplified 30 or 60 dB in total gain with a passband of 30 kHz to 2 MHz, and digitized at a sampling interval of 0.1 μs using a transient recorder (Model 1010 Biomation). The digitized data were stored on floppy disks or on a hard disk drive of a microcomputer and was transmitted to a main computer (DEC VAX-11/750). Most of the software for autoregression analysis used on the main computer were from the Interactive Laboratory System (ILS) package developed by Signal Technology, Inc., Santa Barbara, CA.

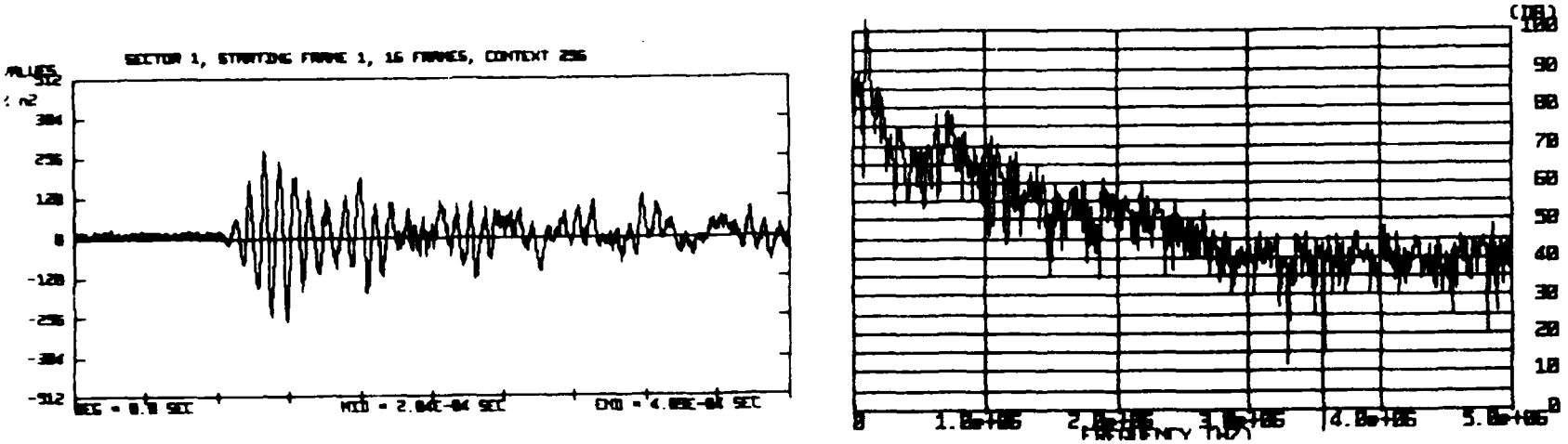

Fig. 1 Waveform AAA and Fourier spectrum of the most significant part.
Full scale: ± 500 µV and 409.6 µs.

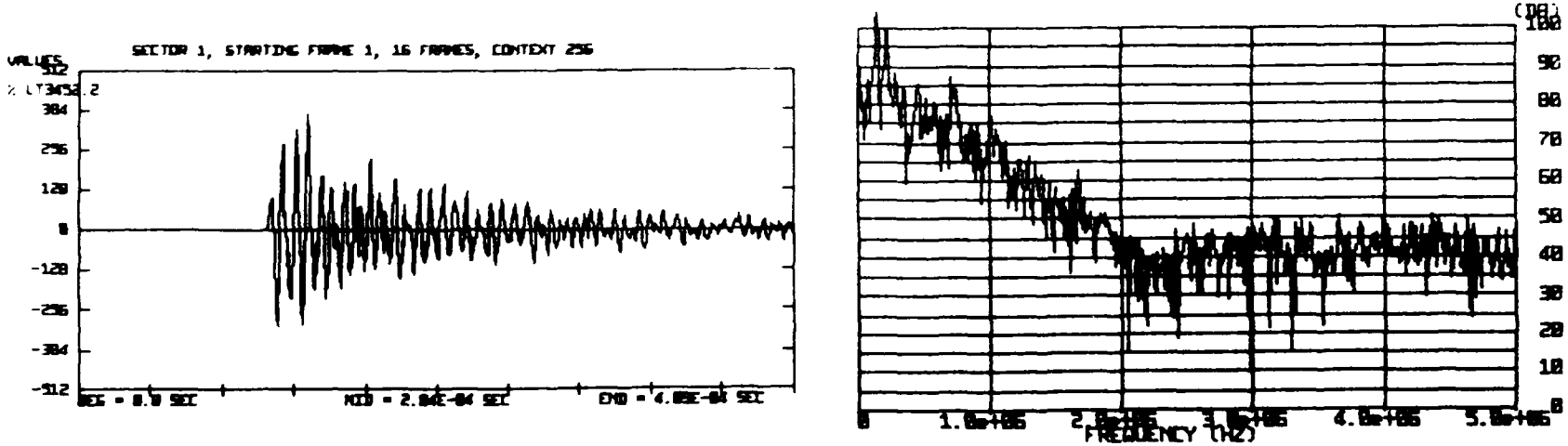

Fig. 2 Waveform JJJ and Fourier spectrum of the most significant part.
Full scale: ± 633 mV and 409.6 µs.

Results and Discussion

Examples of detected AE waveforms are shown in Figs. 1 and 2. They were taken at 85% of the maximum load and at the fracture load, representing crack initiation via tear or shear and cleavage cracking. The Fourier spectrum of the 102μs portion of the main part of the signal is also shown. We computed twelve autoregressive coefficients for each 256 points (this group will be called one frame). For each signal, ten most significant consecutive frames were thus analyzed. As the feature vector for this signal, averaged values of 12 autoregressive coefficients were employed in the subsequent pattern recognition analysis. However, the gain factor was not utilzied, implying that the amplitude data was not included in the present analysis. However, the gain factor was not utilized, implying that the amplitude data was not included in the present analysis.

In this study, we digitized and analyzed 33 waveforms. Distances between all the averaged feature vectors were calculated. Six representative feature vectors were selected as reference since a pattern of groupings emerged. During the pattern recognition analysis, each set of 12 autoregression coefficients was matched against the six reference sets. Figure 3 shows the results. Waveforms AAA to EEE were taken at 86 to 95% of the maximum load and belong to three groups, AAA, BBB and DDD. In this loading region, AE intensity was still low and was just above the background. Ductile crack growth was observed and fractographs showed both tear and shear cracking. Above 95% of the maximum load, AE intensity increased dramatically. Waveforms FFF to HHH were examples of unsaturated signals from this region using a 60 dB preamplifier. These were distributed among the reference groups of FFF, JJJ and LLL. In this high load region, cleavage cracking occurs and these waveforms must be due to cleavage. In taking a second group of waveforms, III through YYY, a 30 dB preamplifier was used. Waveform JJJ was at the maximum load, while those of KKK to YYY were during decreasing load. Most of the second group was classified to the reference JJJ. From the signal intensity and the load level, this is representative of cleavage cracking signals. Two signals, ZAA and ZBB, were taken during the first load reduction. These were classified to BBB and DDD. Since crack face rubbing can be a potential source during the load reduction, the classification by itself cannot be used to identify the type of AE source for ZAA and ZBB. It is also possible that waveforms BBB, CCC and DDD originate from crack face rubbing even though these were detected during load increase. Further study on these aspects is worthwhile.

In the present study, the autoregression coefficients of the AE waveforms were extracted and utilized for pattern classification on the basis of the weighted nearest neighbor decision rule. The autoregression coefficients were found to be adequate for describing variations of observed AE waveforms. Basically, two types of signals were found corresponding to ductile crack and brittle cleavage. The results suggest that real-time recognition of underlying parameters of AE waveforms is feasible.

Acknowledgements

The authors are grateful for a financial support by the Physics Program, Office of Naval Research. We wish also to thank Dr. H. B. Teoh and Mr. Sze-Yuan Lu for their assistance.

References

1. L.J. Graham and R.K. Elsley (1983), "AE Source Identification by Frequency Spectral Analysis for Aircraft Monitoring Application," J. Acoustic Emission, 2 (1/2), 47-55.

2. D. R. Hay, R. W. Y. Chan, D. Sharp and K. J. Siddiqui (1984), 'Classification of Acoustic Emission Signals from Deformatic ı Mechanisms in Aluminum Alloys," J. Acoustic Emission, 3 (3), 118-129

3. M. Ohtsu and Kanji Ono (1984), 'Pattern Recognition Analysis of Magnetomechanical Acoustic Emission Signals," J. Acoustic Emission, 3 (2), 69-80

4. C.H. Chen (1982), Digital Waveform Processing and Recognition, ed. C.H. Chen, CRC Press, Boca Raton, Florida, pp. 5-22, 59-74.

5. R.B. Melton (1982), 'Classification of NDE Waveforms with Autoregressive Models," J. Acoustic Emission, 1 (4), 266-270.

6. K.S. Fu (1982), Applications of Pattern Recognition, ed. K.S. Fu, CRC Press, Boca Raton, Florida, pp. 1-13, 107-119.

7. L.R. Rabiner and R.W. Schafer (1978), Digital Processing of Speech Signals, Prentice-Hall, Englewood Cliffs, NJ.

8. H. B. Teoh (1984), "Acoustic Emission During Deformation and Fracture of A533B Pressure Vessel Steel," Ph. D. Thesis, University of California, Los Angeles.

	AAA	BBB	DDD	FFF	JJJ	LLL
AAA	9					1
BBB		8	2			
CCC		2	8			
DDD		1	9			
EEE	10					
FFF				2	7	1
GGG				3	7	
HHH				1	3	6
ZAA		1	9			
ZBB		6	4			
III				2	8	
JJJ					9	1
KKK	1				9	
LLL	1	1	1		2	5
MMM					7	3
NNN	1				9	
OOO	1				8	1
PPP					8	2
QQQ				1	9	
RRR	2				7	1
SSS					7	3
TTT	1				9	
UUU				1	2	7
VVV				1	9	
WWW					10	
XXX					10	
YYY	1				9	

Fig. 3 Results of pattern classification.

Acoustic Emission Behavior of Metal Matrix Composites

C. Johnson, K. Ono, D. Chellman*
Department of Materials Science and Engineering
University of California, Los Angeles 90024
*Lockheed Corporation, Burbank, CA

INTRODUCTION

Metal matrix composites (MMC's) are displacing monolithic metals and polymer matrix composites in a number of applications. MMC can be used in aerospace and space environments where certain mechanical properties (high temperatures specific strength and stiffness, low creep, low CTE) are important /1/. However, aerospace manufacturers are still concerned with relatively low fracture toughness and strain to failure, brittle stress-strain behavior and limited service experience.

Acoustic emission (AE) detection and analysis can characterize microstructural processes /2/. In this study AE techniques are applied to MMC in order to characterize deformation and fracture mechanics. Such information benefits the user of MMC's in determining their suitability in a particular application.

MATERIALS

Both silicon carbide whisker (SiC_w) and particulate (SiC_p) reinforced aluminum (2124) matrix MMC's were characterized in this study. The SiC_w MMC is produced by ARCO Metals (formerly Silag Division of Exxon Corporation) of the 1982 vintage. It is important to note that material properties have improved significantly within the few years of production history. This material contains 15 and 25% SiC whisker (beta crystalline) reinforcement but includes some nodules (80% SiC_w 20% nodules). The nodules are a process artifact. The fibers range from 0.1 to 1.0 μm in diameter with an average length to diameter ratio of about 4. The other MMC is produced by DWA Composite Specialities, Inc. This material uses 20 and 30% single crystals (alpha structure) of abrasive grade SiC (crushed into fine powder and separated by size) as reinforcement. The SiC_p is in platelet shape with length to thickness ratios of about 1 to 4 and average 5 to 10 μm across.

Similar processes were used to fabricate both SiC_w and SiC_p composites. The reinforcement is mixed with aluminum powder, compacted into billets and hot pressed (typical of powder metallurgy [PM] processes). Both materials arrived in "as extruded" condition. The extrusion process does generate anisotropy in the SiC_w composite (whiskers align in the extruded direction). A special PM material (2124) was processed via the ARCO method for comparison purposes along with ingot metallurgy (IM) processed 2024, 2224 and 2034 alloys.

TEST METHODS

Two floor model Instrons (Model TTL) were used with constant crosshead speed of 8.5 μm/s in room air at ambient temperature for mechanical and AE testing. Suitable dogbone tensile and standard Charpy specimens were machined from the extruded bars for the tensile and three point slow bend tests.

AE parameters collected during both tests included root mean square voltage (V_{rms}), AE and event counts, and amplitude distributions. A piezoelectric transducer [Model MAC175L, Acoustic Emission Technology Corporation (AET)] and a preamplifier with 125-250 kHz (Model 160, AET) were used for all AE measurements. The transducer was acoustically coupled to the gage section of a tensile specimen with viscous resin while wax was used to couple the transducer to the square end of a Charpy specimen. A true rms voltmeter (Model 3400A, Hewlett-Packard) was used to collect the V_{rms} data and a microcomputer based AE analyzer (Model 5000, AET) provided all other AE parameters. In addition, use of a video recorder (Model AV-3650, SONY) enabled continuous waveform observation.

RESULTS AND DISCUSSION

Various heat treatments were examined for any significant differences in acoustic emission. Longitudinal and transverse specimens of the SiC MMC were tested in slow bend and tensile configurations. Solution treatment for the PM material was two hours at 493°C and water quenched. Four hours at 504°C was used for the MMC. A T4 (25°C/96 hours) and three T6 conditions (163°C/48 hours; 177°C./12 hours; 191°C/4 hours) were compared. Results showed no significant differences in AE parameters in the three T6 conditions. Thereafter two conditions, T4 and T6, were compared in detail.

In order to create a meaningful test plan two reinforcement/matrix ratios were acquired for each type of MMC. Orientation and heat treatment conditions complete the test plan.

SEM Observation

Scanning electron microscope (SEM) fractographs of tensile samples reveal primarily ductile fracture appearance (dimples) in all materials (see Fig. 1). Ingot and PM materials showed typical 45° shear failure while the composites showed predominantly flat fracture (with a shear lip). In the SiC_p reinforced MMC, many SiC particles appear on the fracture surface (confirmed by X-ray analysis). The particulate composite surface appears similar to the PM fracture surface (Fig. 1 b and f) where particles are situated in the dimples. Many particles in the PM and IM materials are cracked. The silicon carbide particles remained intact (even in the shear lip area) inferring possible interface failure. The whisker interface is quite strong (three times the matrix shear strength /3/). Fracture origin could be at the particle, its interface, existing voids or other microstructural defects. In SiC_w reinforced MMC, relatively few whiskers were seen indicating that the matrix is favored as fracture path /3/. Pullout holes and whiskers were distinct hardly showing nonuniformity or matrix adherence. Existing voids are inferred as fracture origin but voids may have originated at the ends of whiskers.

AE Behavior

Whisker and particulate composites differ mainly in the amount of continuous emission detected. The SiC_p MMC showed considerable continuous emission after yielding. The whisker composite showed only an increase in burst emission during the test although it never reached significant plastic strain to check for continuous AE.

The PM material (T4 condition) exhibited a low intensity V_{rms} peak (0.5 μV) beyond yield, while both of the composites showed a much higher second peak intensity (10 μV) (see Fig. 2). Low intensity AE activities were also

present in the pre-yield region. A second peak was also displayed in 2XXX series ingot-processed Al alloys. The second peak is not as intense as in the composites (1-3 μV) and has been attributed to inclusion fraction /2/. Comparison of the PM material with SiC_p and SiC_w MMC's indicates that neither of these sources are responsible for the higher second peak V_{rms} intensities of the composites.

The SiC_p MMC in the T4 condition does show a pre-yield V_{rms} peak while it is not found in the T6 condition. Similar behavior is shown in the PM material. This is expected due to increased immobilization of dislocations via aging. Neither condition of the whisker composite showed pre-yield peak. This is related to the high dislocation density and small subgrain size in the matrix resulting from whisker/matrix thermal interaction during processing /3/. Low strain to failures presumably prevented a second peak in V_{rms} to appear, but a magnitude is expected to be lower than that in SiC_p MMC.

An increase in the amount of whiskers (15 wt.% to 25 wt.%) resulted in higher V_{rms} levels. Friction in fiber pullout is another possible AE source mechanism. Longitudinal orientation of the whiskers also correlated with an increase in V_{rms}. The particulate composite, as expected, showed no V_{rms} changes with orientation.

AE Parameters

Throughout all of the tensile tests performed, energy, event counts and AE counts yielded similar information. In addition, rise time data did not vary during the tests. AE count rates and V_{rms} curves were similar in the whisker MMC's. This indicates that the AE is primarily burst type (supported by waveform observation).

Peak amplitude distributions of the particulate composites were tight, low level groupings (34 dB ± 5 dB, re. 1 μV), whereas the whisker composites showed some higher amplitude events in addition. Windowing revealed that in both materials slightly higher amplitude events were detected as V_{rms} increased. The existence of two AE source mechanisms is implied. However, no high amplitude event has been detected in the MMC's unlike glass reinforced composites.

Event durations of the SiC_p MMC were longer than the whisker composite composite (500 vs. 100 μs, on average) which could reflect the size disparity of the two reinforcements.

Three types of acoustic emission have been detected in this study. A pre-yield dislocation motion mechanism was evident in the T4 condition of IM, PM and SiC_p materials. This mechanism was suppressed by aging (T6) or by the significant dislocation-whisker interaction found in the SiC_w MMC. A second peak in IM and PM materials is apparently due to inclusion fracture according to the literature. This peak is masked by another mechanism in the MMC's which produces much higher intensities. This mechanism is characterized by high matrix strains relieved through apparent failures at the interfaces (SiC_p) or interface vicinity (SiC_w).

None of the SiC particulates or whiskers appeared to be broken whereas many inclusions in the IM and PM materials appeared fractured. AE analysis also indicates the absence of high amplitude events. Therefore, MMC fracture is likely to initiate and propagate in the matrix.

ACKNOWLEDGEMENTS

This work was supported by the Physics Program, the Office of Naval Research. We are grateful to Dr. A. P. Divetcha of NSWC, who supplied 25% SiC_w MMC and to Dr. W. Harrigan of DWA Composite Specialty, who provided 20 and 30% SiC_p MMC's.

REFERENCES

1. C. Zweben, 'Metal Matrix Composites Overview," MMCIAC No. 253, Kaman Tempo, Santa Barbara, California, 1984.

2. S. Carpenter and C. Heiple, Fundamentals of Acoustic Emission, ed. K. Ono, University of California, Los Angeles, 1979, pp. 49-104.

3. R.J. Arsenault, Materials Science and Engineering, Vol. 15, 1984, pp. 171-181.

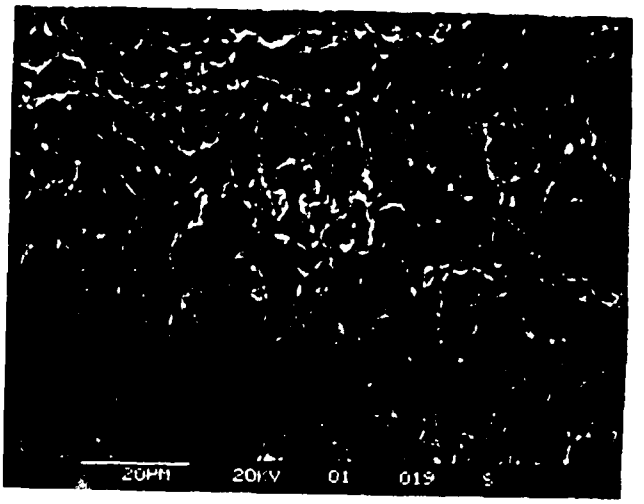
20PM 20KV 01 019 S

(a)

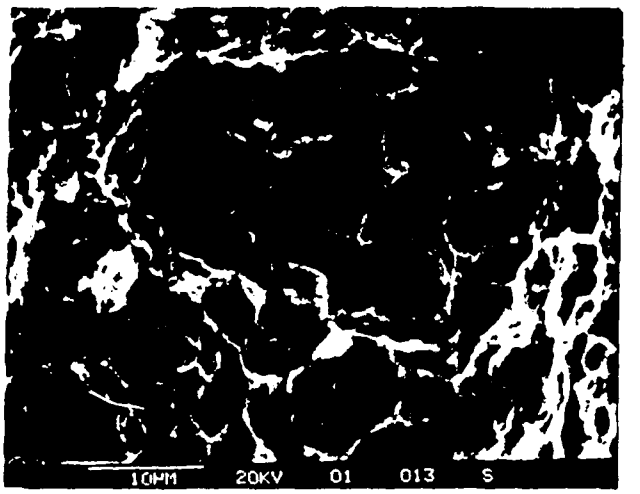
10PM 20KV 01 013 S

(b)

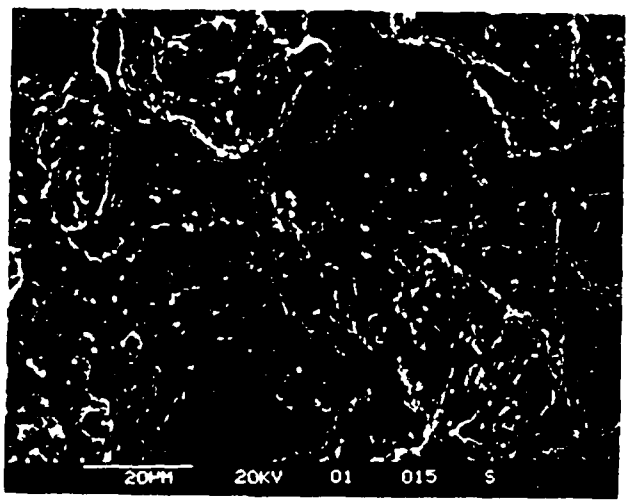
20PM 20KV 01 015 S

(c)

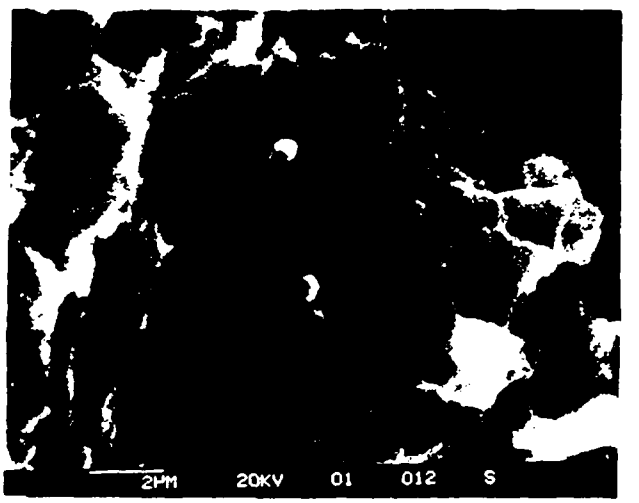
2PM 20KV 01 012 S

(d)

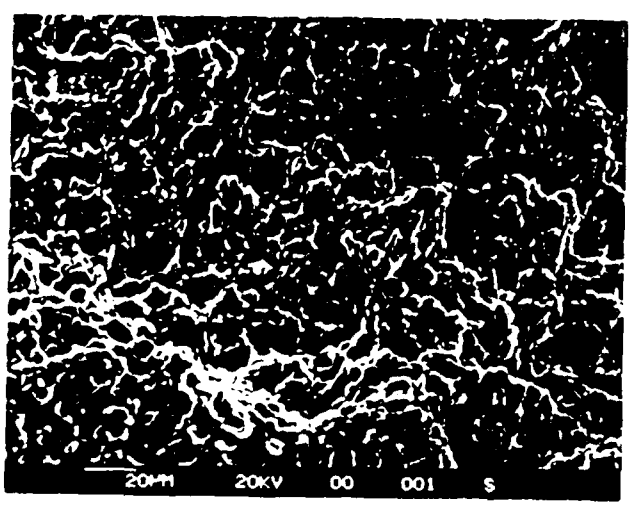
20PM 20KV 00 001 S


4PM 20KV 00 003 S

(e)

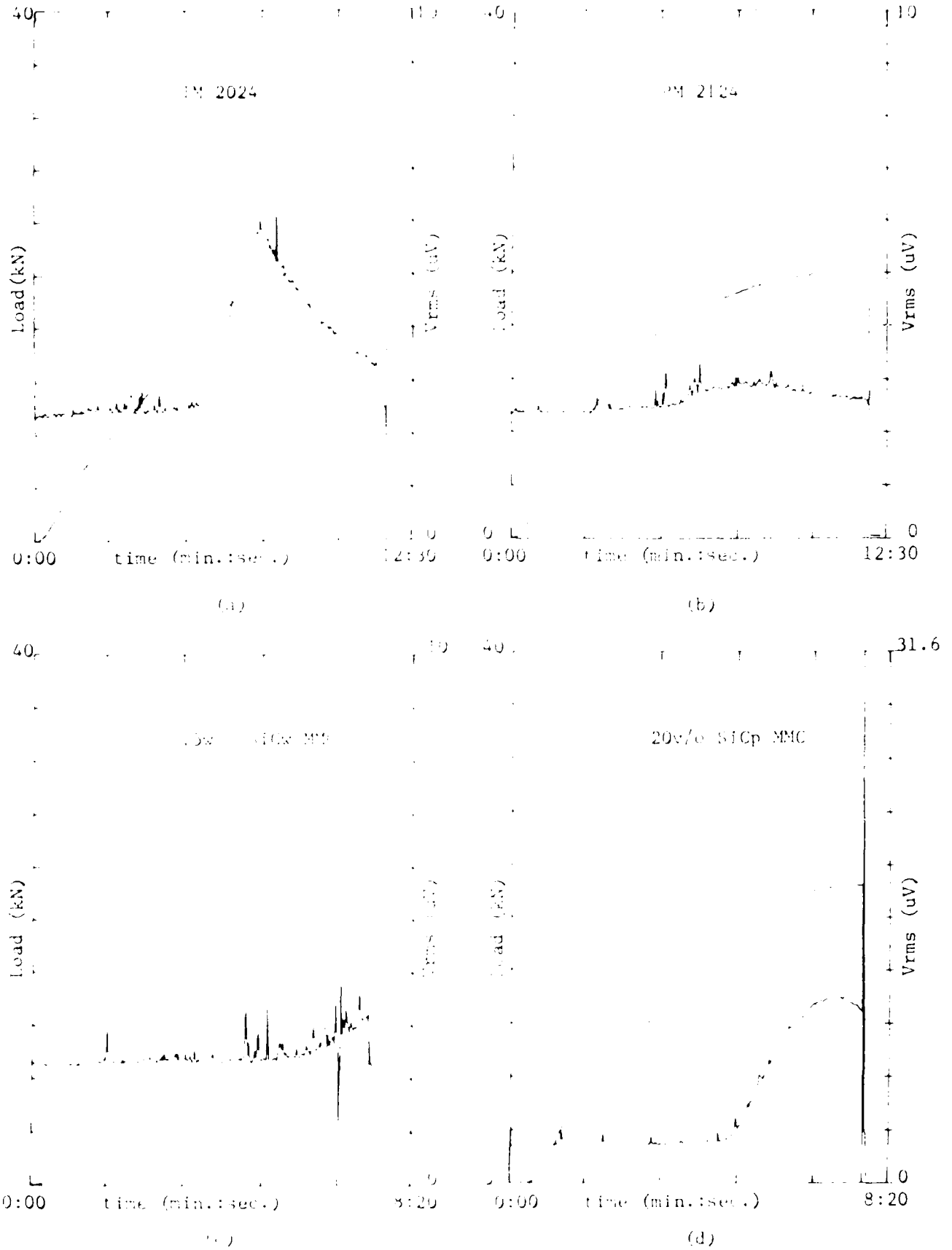

Figure 2, Load and Vrms curves for T6 condition IM 2XXX Al alloy (a), PM 2124 Al (b), whisker composite (c) and particulate composite (d).

Cont'd

Burst-type Emission Behavior of Structural Steels

O. Y. Kwon, I. Roman* and K. Ono
Department of Materials Science and Engineering
University of California, Los Angeles, CA 90024
*Hebrew University of Jerusalem, Jerusalem, Israel.

Introduction

The ductility of steel plates, especially in the thickness (short-transverse) direction, is sensitive to the number, size, shape and distribution of nonmetallic (MnS, in particular) inclusions. Our previous extensive works on a series of low alloy steels have revealed the anisotropic AE behavior which strongly depends on the sulfur content, the rolling ratio of the plate and the heat treatments/1-5/. These studies indicated that the decohesion of MnS incluson/matrix interface is the source of most burst type AE during the tensile loading or fracture of ductile steel members. In recent studies we evaluate the effects of thermal stresses and segregation of impurities on the integrity of the interfaces and consequently on the pre-yield burst emission (PYBE)/6,7/.

The present study was carried out in order to understand the effect of very low sulfur content on PYBE, particularly in conjunction with the amount and shape of inclusions and the presence of particular alloying element(s) in the steel.

Materials and Experimental Procedures

Half size ASTM round tensile samples were machined from two low alloy steel plates (Steels 1 and 2) and a mild steel plate (Steel 3). The S-orientation tensile samples were prepared by friction welding followed by machining. The chemical compositions are given in Table 1.

Steels 1 and 2 were 50mm thick, obtained by rolling ingots of 150mm thickness (67% reduction). The initial and finish rolling temperatures were 1200°C and 1000°C, respectively. The plates were then homogenized at 900°C for 2 hours (as-received condition). No information is available as to the mill practice used for the mild steel plate. Additional heat treatment consisted of austenitization at 905°±5°C for 2 hours in vacuum followed by either cooling at moderate rates in helium atmosphere (as-normalized, N) or quenching into oil followed by tempering either at 550°C (Steels 1 and 2) or at 670°C (Steel 3) for 2 hours (quenched and tempered, QT).

A floor model Instron was used at constant crosshead speed of 0.02 mm/sec for mechanical testing. AE characteristics evaluated during tensile tests were AE event counts, rms voltages and peak amplitude distributions of AE signals. A resonant type transducer (MAC 175L, AET Corporation, Sacramento, California) and a preamplifier (60 dB gain) with 125-250 kHz filter were used for all AE measurements. The transducer was acoustically coupled to the flat end of a sample using viscous resin. AE event count measurement and the amplitude distribution analysis were obtained from a microcomputer-based AE instrumentation (Model 5000, AET Corporation). A true rms voltmeter (3400A, Hewlett-Packard) was employed for the rms voltage measurements.

Results and Discussion

Low alloy steels

Tensile samples were tested in the L- and S-orientations for both the as- normalized (N) and the quenched and tempered (QT) conditions. Tensile properties and AE event counts are summarized in Table 2. Sample orientation and sulfur level had minimal effects on the strength of as-normalized steels but the reduction of area and the tensile elongation of higher sulfur content steel in the S-orientation decreased. The decrease in the ductility parameters was more significant in quenched and tempered samples which also showed a decrease in the strength with increasing sulfur level.

In the N condition, AE behavior of these steels had practically no orientation or sulfur-level dependence. For all N samples, AE started at about 0.5 σ_y. The AE activity was principally continuous and was confined to the vicinity of the yield point where the rms voltage showed a maximum. During yielding and Lueders elongation, the rms voltage level reached 16 μV and also contained some spikes, but rapidly decreased to the background level at the onset of work hardening. These findings are similar to the well-known AE characteristics from plastic deformation due to dislocation motion. spikes on the rms voltage curve during yielding and Lueders elongation can be a clue to minor burst emission activities.

A representative load and AE data for a QT sample is shown in Fig. 1. This is obtained from an S-orientation QT sample of Steel 2. AE activity in this higher strength condition is qualitatively similar to those of N condition, but of a lower intensity. The peak level of rms voltage was below 9 μV and total event counts in Table 2 also manifested the lower AE activity. The decrease in AE activity is due basically to the decrease in continuous emissions since the number of mobile dislocations and their mean free path had been reduced by heat treatment. The total AE event counts in the S-orientation were higher than those in the L-orientation by 30% in Steel 1 and by 100% in Steel 2. Figure 2 shows the peak amplitude distribution of AE data in Fig. 1. While this is a power law distribution rather than Weibull-type distribution, the range of peak amplitude extended to 48 dB (at 1% of the total event counts). In the L- orientation samples, the corresponding value was 40 dB, which agrees with the peak amplitude value expected from the peak rms voltage level. This indicates that AE activities at higher amplitudes are produced by the decohesion of inclusion/matrix interfaces in these tests. It is noteworthy that no pre-yield burst emission was observed in these materials. This was also the case in similar low alloy steels /8/, but in sharp contrast to Ni-containing A533B steels where PYBE was quite prominent /5-7/.

Figure 3 shows the fractogragh of an S/QT sample of Steel 2. The sulfur level in this steel is the typical one through our previous investigations and the fractogragh shows numerous inclusions on the fracture surface. All of them, however, are equiaxed and the size of 1 to 2 μm in diameter. The decohesion of inclusion/matrix interface is a stress-controlled process/4/. Generation of burst-type emissions is more efficient when the broad face of flattened inclusion is normal to the tensile axis. The critical stress to debond the interface is higher for the equiaxed inclusions than for the large flattened oblate ones. The occurrence of burst emissions, therefore, shifted from pre-yield region to general yield region. In addition, since the average size of the inclusions are very small, the peak amplitudes of these burst emissions are reduced and easily covered by higher activities of continuous emissions in the N condition.

Mild steel

The tensile properties and total AE event counts summarized in Table 2 indicate that the ductility parameters depend considerably on the orientation and heat treatment. Note that the S-orientation sample in as-normalized condition failed in elastic region and total counts were also off the expected number. At the correspondingstrain level, the Lsamples showed much lower AE activities than in the Ssamples. The sulfur content is very high and numerous large flattened MnS inclusions were observed on the fracture surface of S-orientation samples. Although the QT samples actually showed some indications of PYBE in the S-orientation, the proportion was not as high as the typical PYBE in the previous studies.

Refering to our previous works on AE behavior of low alloy steels /7/, the presence of nickel appeared to have an important role on the impurity segregations to the MnS inclusion/matrix interface. It is well known that Ni provides the equilibrium segregations of IV-A group elements (essentially P, Sn, Sb, As) to the grain boundary and consequently temper embrittlement in low alloy steels. Sulfur segregates stongly to the MnS inclusion/matrix interface due to its strong interaction with Mn /9/. This enrichment of S at the interface weakened its strength leading to debonding at very low stress, which is detected as PYBE /7/. The results strongly suggest that particular alloying elements(especially Ni) can cause additional effect on the AE behavior of structural steels.

Conclusion

The ductility parameters and AE behavior of strucutral steels becomes almost isotropic when they contain less than 0.001 % S. Effects of MnS inclusions are mitigated due to the reduction of their size and number. Without the addition of Ni as an alloying element, burst emission activities, especially in the preyield region, are suppressed.

Acknowledgement

The authors are grateful for the support of this work by the Physics Program, the Office of Naval Research.

References

1. K. Ono, R. Landy and C. Ouchi (1978), Proc. 4th AE Symp., Int. Tech. Exchange Center, Tokyo, Japan, pp. 4-33 - 4-45.

2. K. Okajima and K. Ono (1980), Proc. 5th Int. AE Symp., Japan Soc. NDI, Tokyo, Japan, pp. 270 - 281.

3. M. Yamamoto, C. Ouchi and K. Ono (1980), Proc. 5th Int. AE Symp., Japan Soc. NDI, Tokyo, Japan, pp. 221 - 235.

4. K. Ono and M. Yamamoto (1981), Mat. Sci. Engr., 47, pp. 247 - 263.

5. H. B. Teoh, I. Roman and K. Ono (1982), Proc. 6th Int. AE Symp., Japan Soc. NDI, Tokyo, Japan, pp. 21 - 30.

6. I. Roman, H. B. Teoh and Kanji Ono (1984), J. Acoustic Emission, 3, pp. 19 - 26.

7. H. B. Teoh, Kanji Ono, E. Kobayashi and I. Roman (1984), J. Acoustic

Emission, 3, pp. 130 - 143.

8. K. Ono, G. Huang and H. Hatano (1976) 'Proc. 8th World Conf. NDT" paper 3K3, Cannes, France

9. M. Guttmann and D. McLean(1979), in 'Interfacial Segregation" (W.C. Johnson and J.M. Blakery, Eds.), ASM, pp. 310 - 338.

Table 1.
Chemical composition of steel plates

	C	Si	Mn	P	S	Cu	Ni	Nb	Sol. Al
Steel 1	0.116	0.24	1.39	0.013	0.0005	0.26	0.22	0.032	0.055
Steel 2	0.120	0.29	1.42	0.011	0.0060	0.26	0.21	0.033	0.037
Steel 3	0.220	0.24	0.78	0.010	0.0160	--	0.13	--	0.04Cr 0.07Mo

Table 2.
Summary of tensile properties and AE event counts

Steel		1		2		3	
Orientation		L	S	L	S	L	S
Yield Strength (MPa)	N	310	312	299	310	277	152
	QT	496	461	426	454	345	345
Tensile Strength (MPa)	T	434	418	414	410	361	-0-
	QT	536	524	500	509	384	386
Reduction of Area (%)	N	80	78.5	77.5	52.9	76	-0-
	QT	78	76	76	32	82	53
Elongation (%)	N	27	30	36	22	37	0
	QT	29	24	24	27	35	27
Total AE evant counts	N	27975	25898	17901	20315	9278	4805
	QT	1925	2574	1964	4065	1429	4531

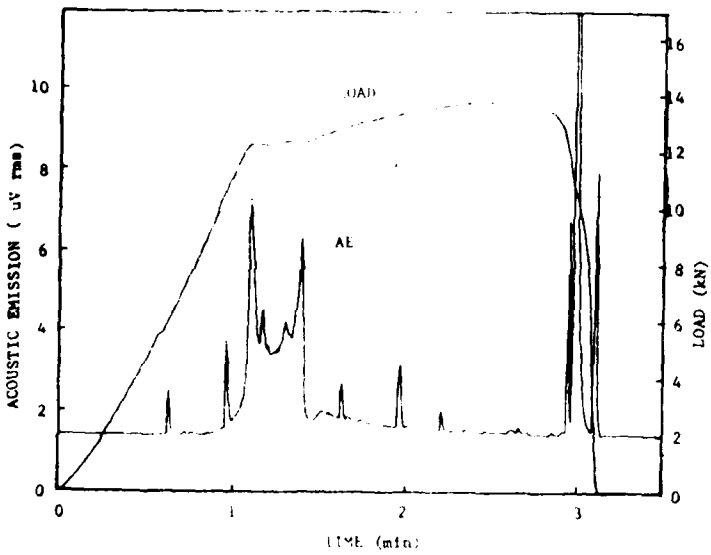

Figure 1 Load and AE data for S/QT sample of Steel 2

Figure 3 Fractograph of S/QT sample of Steel 2

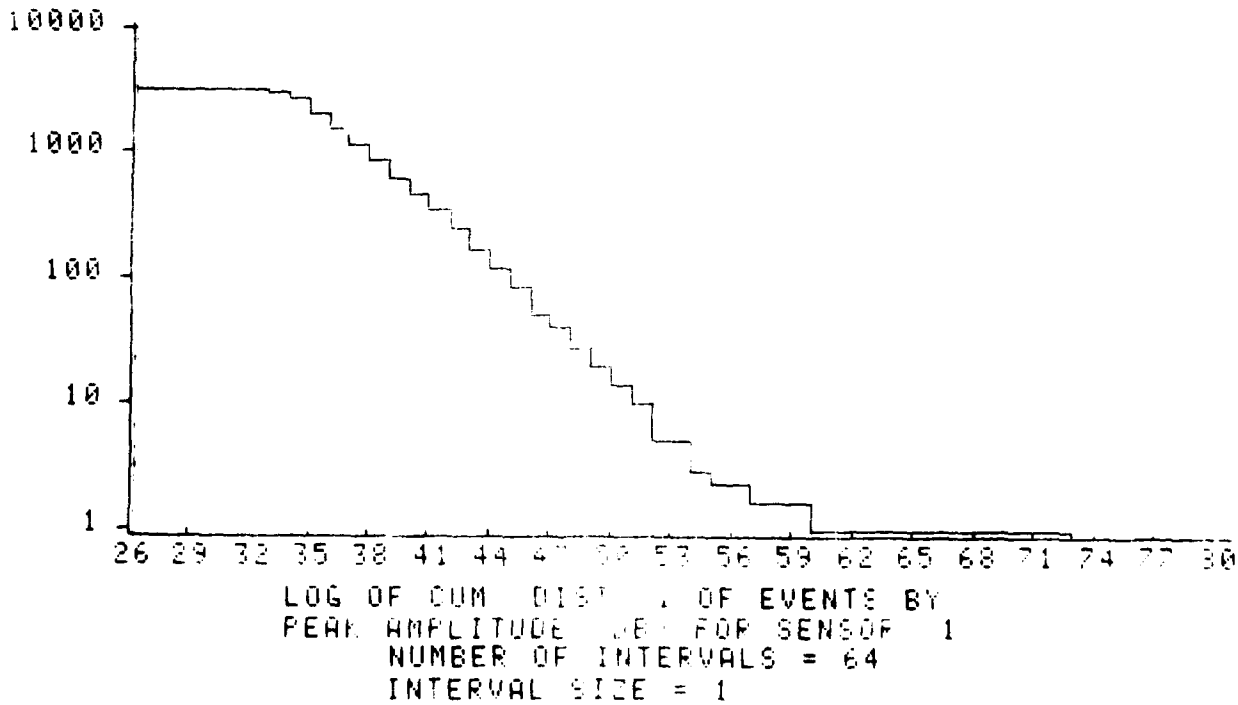

Figure 3 Peak amplitude distribution of AE data for S/QT sample of Steel 2

Acoustic Emission Behavior of an Advanced Aluminum Alloys

I. Roman*, K. Ono and C.H. Johnson

Department of Materials Science and Engineering
University of California, Los Angeles, CA 90024
* Hebrew University of Jerusalem, Jerusalem, Israel.

Introduction

New Al-Li alloys containing up to 3.5 w/o lithium have been subjected to increasing research activities /1/. The interest in these alloys arises from their increased elastic modulus and lower density as compared to conventional Al alloys. Proper heat treatment of these alloys produce a microstructure containing the coherent δ' precipitate phase (Al_3Li) as well as other strengthening phases, such as S' and T_1. These are responsible for significant strengthening of such Al-Li alloys. In the present study, effects of heat-treatment on the acoustic emission (AE) behavior during tensile deformation of an aluminum-lithium alloy have been determined. Origins of AE are discussed in terms of microstructural changes.

Experimental

Longitudinal half-size ASTM standard round tensile samples employed in this study were machined from an extruded 25.4 mm thick plate supplied by Lockheed California Company. Nominal chemical composition of the material, which was supplied in the T3X condition, consisted of 2.5 w/o Cu, 2 w/o Li, 1 w/o Mg and balance Al. Acoustic emission characteristics were evaluated utilizing a microcomputer based system (Model 5000, AET Corp), comprized of 175 kHz resonant transducers (MAC 175, AET), preamplifiers (160, AET) with 125 to 250 kHz passband, main processors and true rms voltmeters (3400A, HP). Samples were tested in an Instron with a strain rate of 2.6×10^{-4}/s. The samples in the as-received condition (T3X) and others (W, T4, T6 and T8X) after heat-treatment were used.

Results and Discussion

The yield and tensile strength increased with aging time for both room temperature (natural aging) and 177°C aged samples. At both aging temperatures, tensile ductility decreased. In all cases, AE signal intensity level reached a maximum prior to yielding and the peak intensity increased with strength level. A typical stress-strain curve and accompanying AE intensity-strain curve are shown in Fig. 1. In all cases, continuous type AE was observed almost from the beginning of elastic deformation. The rms voltage level increased with load and exhibited a prominent peak at about 70% of the yield load. The decrease in rms voltage level during yielding was followed by numerous large AE fluctuations during work hardening which parallel stress level serrations and which increased with aging time. This post yielding AE activity is clearly indicative of dynamic strain-aging. It is more pronounced for the naturally aged samples, and reflects the presence of mobile solute atoms.

The effect of aging time on both the yield and tensile strength of samples aged at 24°C and 177°C are shown in Fig. 2. The effect of aging time on the magnitude of the peak rms voltage level is also shown in Fig. 2. It is evident that for the two aging treatments both the strength and magnitude of the peak rms voltage level of AE increased with aging time.

The observed increase in AE with aging time and dynamic strain aging are unusual for precipitation hardened aluminum alloys. Studies of AE in precipitation strengthened aluminum alloys /2,3/, such as 7075, 2024 and 2219, have shown that the magnitude of the peak AE was greatest in the solution-treated condition and was lowered by precipitation.

Heiple et al. /3/ have observed increased AE activities with aging for JBK-75 (modified A286) and KHB austenitic stainless steels and Incoloy 903. They have explained the different dependency of AE on aging time for the two groups (aluminum alloys vs. iron or nickel alloys) by virtue of the nature of dislocation-precipitate interaction. In the aluminum alloys, cross slip is possible and dislocations tend to bypass precipitates rather than form pile-ups. As precipitates limit the motion of dislocations, they lead to decreased AE. Conversely, cross slip is more difficult in the iron-base or nickel alloys. In this case, the dislocation shears the precipitates that serve as breakable pins which lead to dislocation avalanches and thereby increased AE. Such differences were attributed to the difference in both Young's modulus and stacking fault energy of the two types of alloys.

The δ' precipitates in the Al-Li alloy are shearable and hence the increased AE with aging appears to be related to shearing of the precipitates. However, the explanation by Carpenter and Heiple as to the origin of the dislocations-precipitate interaction does not hold in this case. The stacking fault energy of Al-Li alloys may be lower than in other commercial aluminum alloys but not as low as in stainless steels and Young's modulus is only about 10% higher than other Al alloys. It seems that the different behavior originates from the nature of the precipitates. It is significant that many alloys with increased AE activities in the aged conditions are strengthened by **coherent** and **ordered** precipitates. In the case of the iron or nickel alloys those are coherent ordered γ' ($Ni_3(Al,Ti)$) precipitates /4/ and in the case of Al-Li those are coherent and ordered δ' precipitates. In these alloys, cross slip is not observed due to the anti-phase boundary in sheared precipitates and dislocation pile-ups are commonly observed. However, these are not the only type of precipitates accompanied by increased AE intensity. In fact, S' phase generates substantial strengthening in Mg-containing Al-Li alloys as in the present case. Masuda /5/ studied several precipitation hardened alloys and found AE behaviors in Cu-Co, Cu-Ti, Cu-Be and Cu-Ni-Si alloys in part analogous to the present findings. In these alloys, some of the precipitates are coherent and shearable, but not ordered. Yet, early stages of aging often were accompanied by the increase in AE intensity. He proposed to relate AE to individual dislocation unpinning processes. His proposal correlates the number of unpinning events to AE intensity. However, this model cannot explain the AE behavior of alloys strengthened by coherent and ordered precipitates. In such alloys, the volume fraction of precipitate phase remains nearly constant and the coarsening of the precipitates contributes to the observed strengthening. That is, the number of the precipitates decreases with the progress of aging. Thus, these models cannot explain the observed AE behavior of the Al-Li alloy.

In shearing coherent precipitates, it is expected that largest particles offer the strongest resistance and a group of dislocations are held against them. When such particles are sheared, a large slip step is generated, producing a strong AE event as many dislocations follow the lead dislocation. This is expected to be one of possible mechanisms. Another is when coherent particles are repeatedly sheared, these eventually lose the resistance against dislocation motion. Where a large area is cleared of obstacles, dislocations can move easily and become a strong source of AE. While these mechanisms need to be developed further, they can provide the basis for explaining the AE behavior of precipitation hardened materials.

The dynamic strain aging observed is unusual for a precipitation hardened alloy. This behavior stems most likely from the localized nature of slip in this alloy. After shearing of the precipiates on one slip plane, the dislocations interact with the mobile solute atoms, bringing about the dynamic strain aging.

Summary

The present study was carried out in order to understand acoustic emission characteristics of new aluminum alloys for aircraft applications. These alloys contain lithium and have high stiffness and strength at lower density. Tensile samples along the extrusion direction were solution heat-treated and aged at 24 and 176°C with or without stretching immediately after solution treatment. In all cases, AE signal intensity reached a maximum before yielding and increased with strength level. In work-hardening region, dynamic strain aging was observed, reflecting the presence of mobile solute atoms. Correlation of strength, ductility and AE behavior is reported. Possible mechanisms of unusual AE-strength relation are discussed in terms of precipitating phases present.

Acknowledgements

The authors are grateful for the support of this research by the Office of Naval Research, Physics Program, and to David Chellman of Lockheed California Company for supplying the sample material.

References

1. T.H. Sanders, Jr. and E.A. Starke, Jr., "Overview of the Physical Metallurgy in the Al-Li-X Systems," in Al-Li Alloys II, Proceedings of the 2nd Intl Al-Li Conf., Monterey, CA, April 12-19, 1983, Metallurgical Society of AIME, pp. 1-15.

2. S.H. Carpenter and C.R. Heiple, "Acoustic Emission Generated by Dislocation Mechanisms during the Deformation of Metals," in Fundamentals of Acoustic Emission, ed. K. Ono, University of California, Los Angeles, 1979, pp. 49-104.

3. C.R. Heiple, S.H. Carpenter, and M.J. Carr, "Acoustic Emission from Dislocation Motion in Precipitation-Strengthened Alloys," Metal Science 15 (1981) 587-598.

4. R.F. Decker, "Strengthening Mechanisms in Nickel-Base Superalloys," in Steel Strengthening Mechanisms, AMAX/Climax Molybdenum Co., Ann Arbor, 1969, pp. 147-170.

5. J. Masuda, The Fifth Internatinal AE Symp., eds. M. Onoe et al, JSNDI, Tokyo, 1982, pp. 304-317.

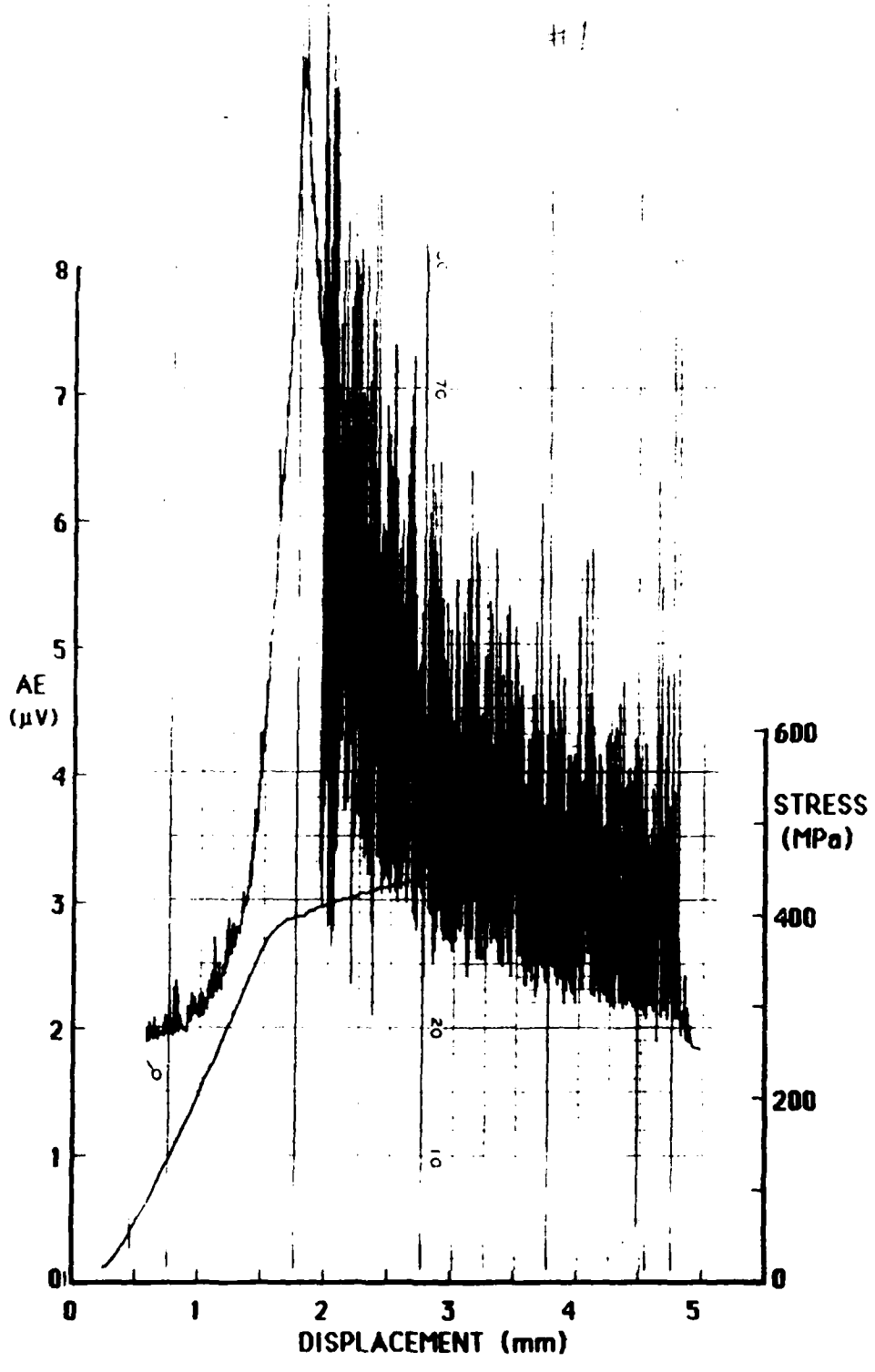

Figure 1. A typical stress and AE intensity vs. displacement curves for Al 2.5 Cu - 2 Li - 1 Mg alloy (T8 condition).

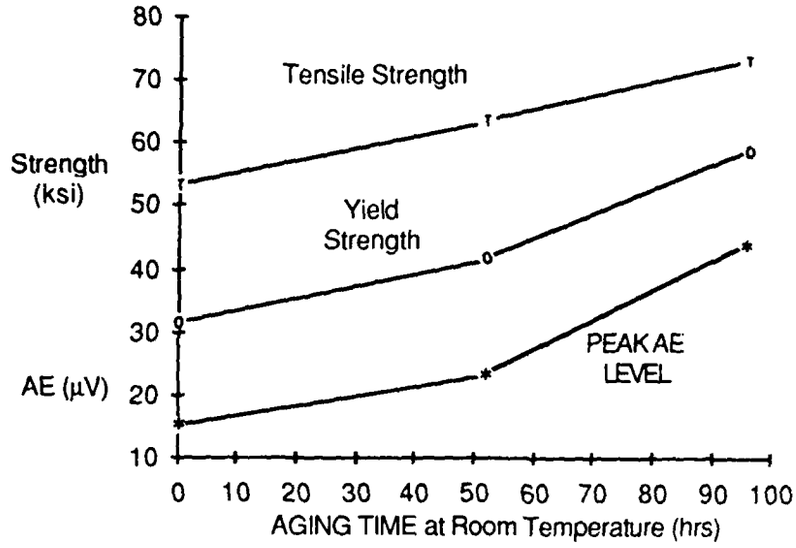

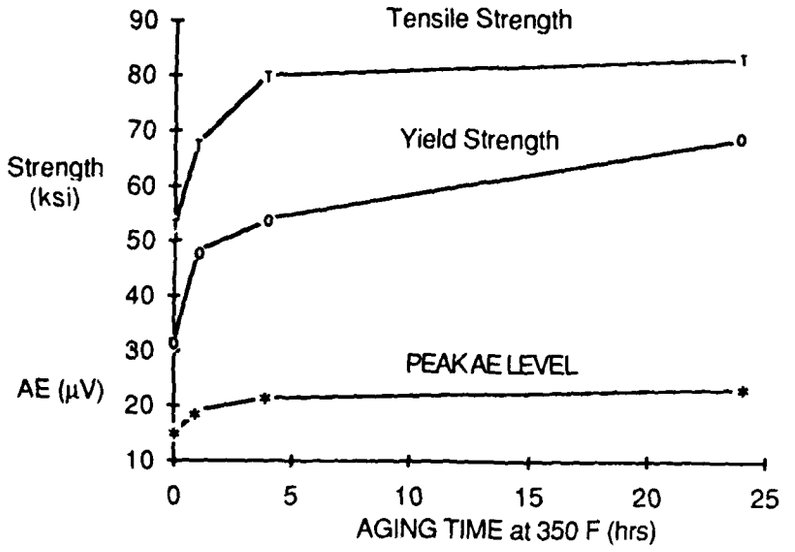

Figure 2. Tensile and yield strength and peak AE level at yielding as a function of aging time (room temperature aging; top; 350°F aging: bottom).

END

FILMED

11-85

DTIC